Clinical Radiology 74 (2019) 547–554

Contents lists available at ScienceDirect

Clinical Radiology

journal homepage: www.clinicalradiologyonline.net

The value of quantitative CT texture analysis in differentiation of angiomyolipoma without visible fat from clear cell renal cell carcinoma on four-phase contrast-enhanced CT images

M.-W. You [a], N. Kim [b], H.J. Choi [c,*]

[a] Department of Radiology, Kyung Hee University Hospital, Seoul, South Korea
[b] Department of Convergence Medicine, Biomedical Engineering Research Center, University of Ulsan College of Medicine, Asan Medical Center, Seoul, South Korea
[c] Department of Radiology, Seoul National University College of Medicine, and Institute of Radiation Medicine, Seoul National University Medical Research Center, Seoul, South Korea

ARTICLE INFORMATION

Article history:
Received 3 April 2018
Accepted 20 February 2019

AIM: To investigate the diagnostic performance and usefulness of texture analysis in differentiating angiomyolipoma (AML) without visible fat from clear cell renal cell carcinoma (ccRCC) on four-phase contrast-enhanced computed tomography (CECT).

MATERIALS AND METHODS: Seventeen patients with AML without visible fat and 50 patients with ccRCC of size ≤4.5 cm who had also undergone preoperative four-phase CECT were included in this study. The histogram, grey-level co-occurrence matrix (GLCM), and grey-level run length matrix (GLRLM) were evaluated. Sequential feature selection (SFS) and support vector machine (SVM) classifier with leave-one-out cross validation were used.

RESULTS: Using the SFS and SVM classifiers, five texture features were selected; mean (unenhanced), standard deviation (unenhanced and excretory), cluster prominence (nephrographic), and long-run high grey-level emphasis (corticomedullary). Diagnostic performance of the five selected texture features for all CT phases was as follows: 82% sensitivity, 76% specificity, 85% accuracy, and 85 area under the receiver operating characteristic curve (AUC). In the subgroup analysis, the AUCs of each phase were significantly >0.5 ($p<0.05$). In the pairwise comparison of AUCs between four phases, there were no significant differences between the four phases except the unenhanced and corticomedullary phases ($p=0.015$), i.e., the unenhanced phase showed slightly higher AUC than the corticomedullary phase.

CONCLUSIONS: Texture analysis of small renal masses (≤4.5 cm) on four-phase CECT can accurately differentiate AML without visible fat from ccRCC and showed good diagnostic performance for both the unenhanced and enhanced phases.

* Guarantor and correspondent: H. J. Choi, Department of Radiology, Seoul National University College of Medicine, and Institute of Radiation Medicine, Seoul National University Medical Research Center, 101 Daehangno, Jongno-gu, Seoul 110-744, South Korea. Tel.: +82 2 970 8651; fax: +82 2 970 8346.
E-mail address: hjcbnbc@naver.com (H.J. Choi).

https://doi.org/10.1016/j.crad.2019.02.018
0009-9260/

Introduction

Angiomyolipoma (AML) is the most common solid benign renal tumour.[1] Accurate preoperative differentiation of AML from renal cell carcinoma (RCC) is often challenging, and approximately 2–6% of solid masses that are surgically excised from the kidney are AMLs.[2] The diagnosis of AML is based on the detection of adipose tissue within a renal mass using computed tomography (CT) and magnetic resonance imaging (MRI); however, approximately 4.5% of AMLs may not show identifiable macroscopic fat and are indistinguishable from RCCs on imaging studies alone.[3] These are called AMLs without visible fat, which contain <25% fat content per high-power field at the histopathological level or non-visible fat on unenhanced CT.[4] Many previous reports have studied determinative factors for differentiation of AML without visible fat from RCC using CT,[1,5–8] MRI[2,4,9–13] and contrast-enhanced ultrasound (CE US)[14]; however, Yang *et al.*,[7] demonstrated that both AML without visible fat and clear cell RCC (ccRCC) show early strong enhancement and a washout pattern. In addition, there are controversial reports about the usefulness of opposed-phase and in-phase gradient-echo MRI images for differentiating AML from RCC.[2,9] Although low signal intensity (SI) on T2-weighted[2,10,11] or fat-suppressed T2-weighted MRI images[4,12] was suggested as one of the characteristics of AMLs, this is not a specific finding for AML without visible fat.

A homogeneous enhancement pattern has been reported to be one of the important features of AML without visible fat[5–7]; however, homogeneity is evaluated by visual analysis, leading to concerns over interobserver agreement and reproducibility. Considering the recent increase in the detection rate of small renal masses (<4 cm), objective determination of the homogeneity or heterogeneity of small renal masses would be more challenging.[2,15]

Texture analysis is an emerging technique used to measure tissue heterogeneity in digital images that is not perceptible to human vision.[16] This computer-assisted technique provides objective measurements of heterogeneity based on grey-level intensity and the position of the pixels within an image.[17] Recent studies presented promising results in the diagnosis, response assessment, and prediction of prognosis and treatment in the field of oncology[18–22]; however, to the authors knowledge, there are few reports applying texture analysis to differentiate renal masses such as AML from RCC.[23] In addition, previous studies have focused on non-enhanced CT texture. The present study attempted to investigate the diagnostic performance and usefulness of quantitative CT texture analysis in the differentiation of AML without visible fat from ccRCC using four-phases CT.

Materials and methods

Patients

This retrospective study was approved by the institutional review board of Asan Medical Center and the requirement for informed consent was waived. From November 2008 to December 2010, an internal Pathology Department database was searched for histopathologically confirmed cases of AML and ccRCC. Among 39 patients with AML, consecutive cases were selected with the following inclusion criteria: (1) individuals who underwent preoperative four-phase CECT, consisting of unenhanced, corticomedullary, nephrographic, and excretory phases; (2) tumour size between 10 and 45 mm; and (3) no visible fat within the mass on unenhanced CT. The exclusion criteria were (1) epithelioid AML; (2) AML with visible fat on unenhanced CT; (3) tumour size >45 mm or <10 mm; and (4) use of CT protocols other than four-phase CECT or outside CT. The lower limit of the lesion size was defined as 10 mm, because lesions <10 mm are too small to draw detectable regions of interest (ROIs) to obtain meaningful information from the software's spatial filters. According to the definition of a small renal mass, the upper margin of lesion size should be 40 mm, but it was adjusted the upper margin to 45 mm according to the maximum size of included AMLs without visible fat in the present study. Among the 661 consecutive patients with histopathologically confirmed ccRCC during the same period, to achieve equivalent weighting compared with AML, 180 patients with ccRCC were selected by random selection using Excel (Microsoft Office Excel 2007, v12.). Inclusion and exclusion criteria were similar to those of AML. Cases of cystic RCC were also excluded because the solid portion was too small to draw detectable ROIs. Finally, 17 patients with AMLs without visible fat (five men and 12 women; mean age, 47.5±2.8 years; age range, 31–69 years) and 50 patients with ccRCC (37 men and 13 women; mean age, 53.3±1.6 years; age range, 28–75 years) were included in the study (Fig 1).

CT examination protocol

All CT examinations were performed with one of the following three 16- or 64- channel multidetector row helical CT machines: Somatom Sensation 16, Somatom Definition 64 dual source (Siemens Medical Solutions, Forchheim, Germany; n=11 AML patients, n=33 ccRCC patients), and

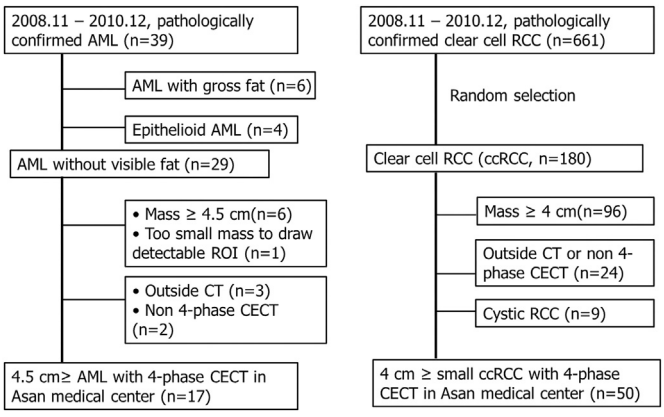

Figure 1 Flow chart of patient selection in the two groups.

Lightspeed VTC (GE Medical Systems, Milwaukee, WI; n=6 AML patients, n=17 ccRCC patients). Imaging parameters for Somatom 16/64 MDCT were as follows: 120 kV; 55 mAs on pre; 180 mAs on arterial; 100 mAs on portal for online dose modulation system (Caredose 4D); 43 mAs on the delayed phase; 16×0.75 mm or 64×0.6 mm detector collimation; pitch=1; 0.5 second rotation time; reconstruction at 3 mm section thickness and 3 mm section intervals. The parameters for Lightspeed VTC were as follows: 110 mA on pre; 100–360 mAs on arterial; 100 mA on portal for the automatic dose modulation system (Auto and Smart mA); and 85 mA on the delayed phase. The reconstruction algorithm was all standard mode, that is, filtered back projection and post-processing was not applied after generation of CT images.

All images were acquired using kidney CT (n=16 AML patients, n=45 ccRCC patients) or urography CT protocols (n=1 AML patients, n=5 ccRCC patients) consisting of four dynamic phases as follows: after acquisition of unenhanced images, ioversol (Optiray 320; Mallinckrodt; USA) 120–140 ml for kidney CT and iobitridol (Xenetix 300; Guerbet; France) 120–140 ml for urography CT was infused through a peripheral intravenous line at 3 ml/s and an additional 200 ml saline was flushed at 2 ml/s for urography CT. The bolus-tracking technique was applied with the trigger threshold set at 100 HU aortic enhancement and after a post-trigger delay of 10–12 seconds, images in the corticomedullary phase were obtained. Nephrographic and excretory phases were acquired at 90 seconds and 4 minutes, respectively, after intravenous injection of contrast media.

Texture analysis of AMLs and clear cell RCCs

The most appropriate CT images covering the renal mass on each unenhanced, arterial, portal, and delayed phase were selected and transferred to be stored as DICOM images. These DICOM images were retrieved and loaded to aMRICro program (MRICro, v1.40, Neuropsychology Lab, Columbia SC, USA) for manual determination of ROIs for textural analysis. Using this program, one radiologist (M.W.Y., with 6 years of experience with abdominopelvic CT) manually drew ROIs within the renal masses. The ROI was carefully drawn to avoid crossing the lesion boundary; thus, only the mass contour was included and analysed (Fig 2). The ROI of each renal mass was drawn at the largest diameter of the lesion on axial section two dimensionally. After acquiring pixel values of the mass, the in-house software Matlab 2013b (MathWorks, Natick, MA, USA) was used to evaluate a total of 35 quantitative texture parameters on each ROI in each of the four phases.

Statistical methods for texture analysis were used and 35 texture parameters were analysed by classifying them into three categories: (1) histogram features including mean, standard deviation, skewness, kurtosis; (2) 20 grey-level co-occurrence matrix (GLCM) features including entropy,

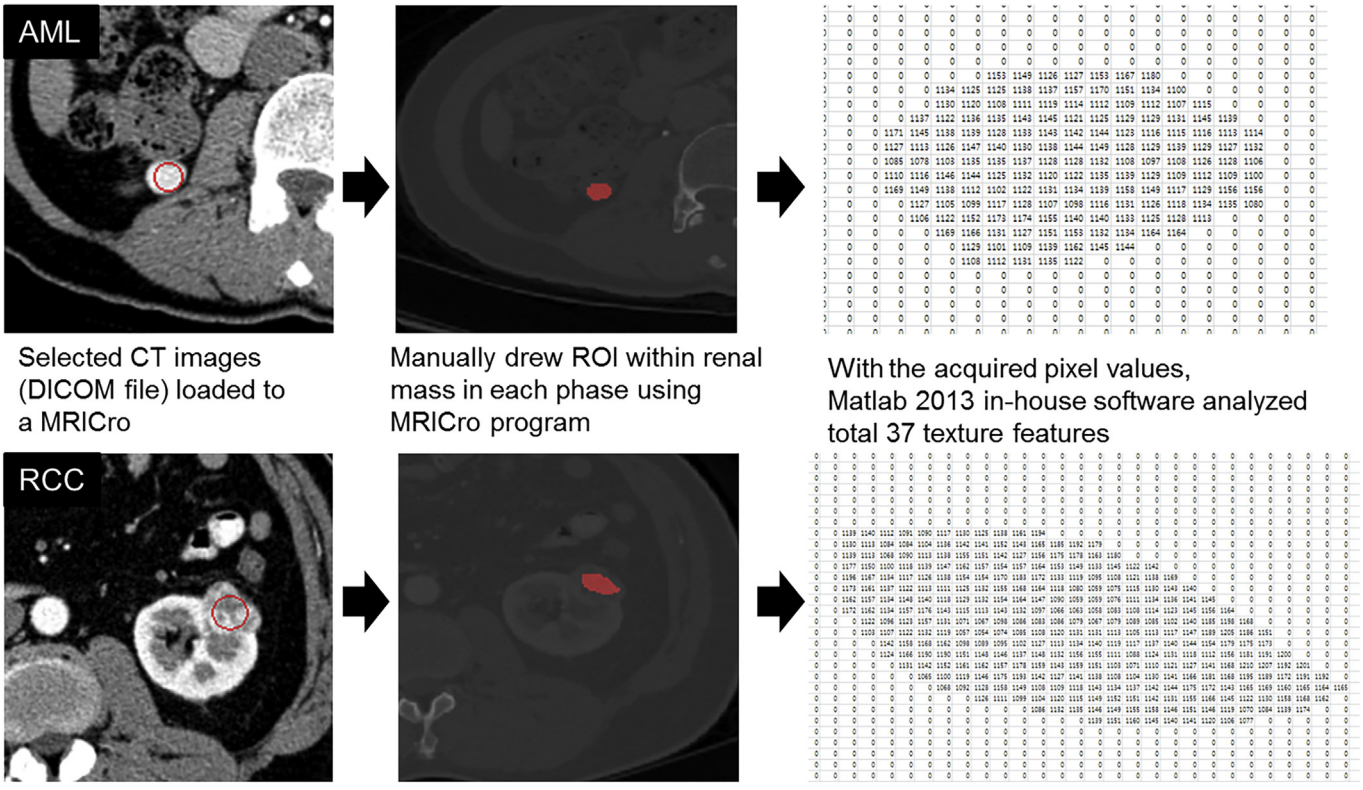

Figure 2 Manual determination of ROIs on axial CT images in each phase of the 17 AMLs without visible fat and 50 ccRCC.

energy, contrast, homogeneity, dissimilarity, and uniformity; and (3) 11 grey-level run length matrix (GLRLM) features, including run length and emphasis.[24]

A GLCM method is a second-order statistic that analyses the spatial grey level dependence of two adjacent pixels.[25] GLRLM is a higher-order statistic that analyses three or more pixels occurring at specific locations relative to each other.[25] The analysed texture features are listed in Table 1.

Sequential forward feature selection and support vector machine classification

In order to select the optimal feature subset of automated classification from a 140-feature set, sequential forward feature selection (SFFS) was applied. It starts with an empty set and adds one feature that increases classification accuracy at each step. The estimate of the quality of the selected subsets usually depends on the training/testing split of the data.[26]

A support vector machine (SVM) classifier was used to classify each ROI into either AML or ccRCC. In each experiment, a leave-one-out cross-validation scheme was applied to evaluate the classifier's validity due to the lack of available data to perform the usual training. Leave-one-out cross-validation is a special case of k-fold cross-validation in that k equals the data size. The available data are divided into k disjoint sets; k models are then trained, each on a different combination of k−1 partitions and tested on the remaining partition.[27] Subgroup analysis was also performed in each phase of CECT.

Table 1
List of the 35 quantitative texture features analysed.

Category	Descriptor	Dimension
Textual eatures	Histogram	Mean
		Standard deviation (SD)
		Skewness
		Kurtosis
	Grey level co-occurrence matrix (GLCM)	Autocorrelation
		Contrast
		Correlation
		Cluster prominence
		Cluster shade
		Dissimilarity
		Energy
		Entropy
		Homogeneity
		Maximum probability
		Sum of squares: variance
		Sum average
		Sum variance
		Sum entropy
		Difference variance
		Difference entropy
		Information measure of correlation 1
		Information measure of correlation 2
		Inverse difference normalized (INN)
		Inverse difference moment normalized
	Grey level run length matrix (GLRLM)	Short run emphasis,
		Long run emphasis,
		Grey-level non-uniformity,
		Run length non-uniformity
		Run percentage
		Low grey-level run emphasis
		High grey-level rum emphasis
		Short run low grey-level emphasis
		Short run high grey-level emphasis
		Long run low grey-level emphasis
		Long run high grey-level emphasis

Statistical analysis

All statistical analyses were performed using MedCalc ver. 14.10.2 (MedCalc Software, Mariakerke, Belgium). Patient age and mean tumour size of the two groups were compared using the independent sample *t*-test and the distribution of patient gender was compared using the Pearson X^2 test. Texture features of the two groups were analysed using the independent sample *t*-test in the univariate analysis. To identify significant texture variables that could be used in differentiating AMLs from ccRCCs, multivariate analysis using sequential feature selection (SFS) was performed. Receiver operating characteristic (ROC) curve was generated from the results of the SVM classifier with leave-one-out cross-validation. The diagnostic performance of texture analysis in each and the combined four CT phases was evaluated using AUC values, and pairwise comparison was performed between the four CT phases using the *z* statistic. All statistical tests were two-sided and differences were considered statistically significant if $p<0.05$.

Results

Clinical features of the AML and ccRCC groups

Clinical features of AML and ccRCC are summarised in Table 2. The AML group showed a lower mean age (47.53±2.76 versus 53.32±1.62 years) and female dominance (70% versus 26%) compared with those of ccRCC group. The mean lesion diameter was greater in the ccRCC group (24.66±1.14 versus 21.06±11.32 mm). The tumours showed no difference in the distribution of location. Most AMLs were confirmed by biopsy whereas most ccRCCs were confirmed by nephrectomy.

Selected texture features in four-phase CECT

The results of univariate analysis with a *t*-test are presented in Electronic Supplementary Material Figs. S1 and S2. Among the 140 texture features in the four phases of CECT, 42 features were significantly different between AML without visible fat and ccRCC. In the unenhanced phase (phase 1), "mean" was the only significantly different feature between AML and ccRCC lesions ($p<0.001$).The "mean" indicates the average pixel value, such as the intensity/brightness of a region,[17] and this "mean" in the AML group was significantly higher than that in the ccRCC group in the unenhanced phase. In

Table 2
Clinical features of 17 patients with angiomyolipomas (AML) without visible fat and 50 patients with clear cell renal cell carcinomas (ccRCC).

	AML (n=17)	ccRCC (n=50)	p-Value
Age	47.53±2.76	53.32±1.62	<0.0001
Sex (M:F)	5:12	37:13	0.002
Mean lesion diameter (mm)	21.06±11.32	24.66±1.14	0.03
	1–2 cm: 10	1–2 cm: 14	
	2–3 cm: 2	2–3 cm: 21	
	3–4.5 cm: 5	3–4.5 cm: 15	
Location of tumour	Upper 8	Upper 13	NA
	Interpolar area 5	Interpolar area 23	
	Lower 4	Lower 14	
CT vendor	GE 6	GE 17	NA
	Siemens 11	Siemens 33	
Method of operation	Partial nephrectomy 0	Partial nephrectomy 11	NA
	Radical nephrectomy 3	Radical nephrectomy 36	
	Biopsy only 14	Biopsy only 2	

NA, not applicable.

the corticomedullary phase (phase 2), 19 texture features, including standard deviation [SD], energy, entropy, homogeneity, and dissimilarity were significant features in differentiating the two groups. Higher values of entropy and dissimilarity and lower values for energy and homogeneity were found in the ccRCC group, indicating that ccRCCs are more heterogeneous than AMLs without visible fat. Seven and 15 texture features were significant in the nephrographic (phase 3) and excretory phase (phase 4), respectively.

The selected texture features in the multivariate analysis using SFS are listed in Table 3. These selected texture features were different from those in univariate analysis in each dynamic phase. In the unenhanced phase (phase 1), "mean" was also a significant feature along with SD and short-run emphasis (SRE). SRE is a measure of the distribution of short runs, and this feature is expected to be large for fine textures[28]; therefore, this feature was larger in the AML group. In the corticomedullary phase (phase 2), SD and cluster prominence, which is one of the GLCM-based texture features, were the significant features. In the nephrographic phase (phase 3), SD, entropy, sum entropy, and the information measure of correlation 1 were the selected features. Entropy measures the disorder or complexity of an image[29]; therefore, a body with a more complex and non-uniform texture, such as RCC, would show higher entropy. In the excretory phase (phase 4), SD, kurtosis, and low grey-level emphasis (LGRE) were selected. LGRE measures the distribution of low grey-level values,[28] and this is expected to be large for images with low grey-level values, which is correlated with AML than ccRCC.

The finally selected five features of all CT phases were mean (unenhanced), SD (unenhanced and excretory), cluster prominence (nephrographic), and long-run high grey-level emphasis (LRHGE; corticomedullary). LRHGE measures the combined distribution of long runs and high grey-level values.[28] This feature is expected to be large for images with many long runs and high grey-level values, which is correlated with ccRCC than AML.

Diagnostic performance of texture analysis in the differentiation of AML without visible fat from ccRCC

The diagnostic performance of texture analysis from an SVM classifier are listed in Tables 4 and 5, and the generated ROC curves in each of the four phases of CECT are presented in Fig 3. The AUC values of the four CT phases were all >0.5 (0.859 unenhanced phase, 0.715 corticomedullary phase, 0.781 nephrographic phase, 0.747 excretory phase; $p<0.05$). The combined AUC of all four phases was 0.853, which was also significantly >0.5 ($p<0.001$). Among individual phases, the unenhanced phase showed the highest accuracy (85.1%; AUC, 0.859), compatible with those of all four phases combined (85.1%; AUC, 0.853). The other three enhanced phases, corticomedullary, nephrographic, and excretory phases, also showed reliable diagnostic accuracy (79.1–83.6%).

In the pairwise comparison of AUC values between the four CT phases, there were no significant differences between the CT phases except for the unenhanced and corticomedullary phases. The AUC of the unenhanced phase was significantly higher than that of the corticomedullary phase ($p=0.015$).

Discussion

Previous studies have reported that attenuation measurement histogram analysis would be useful to differentiate AML from RCC[30]; however, this approach has shown limited application with discrepant results in various studies. The present texture analysis with 140 texture features of three categories using all four CT phases allowed reliable differentiation of AML without visible fat from ccRCC and more detailed analysis than attenuation measurement histogram analysis.

Texture analysis of the CT images was performed to assess the intratumoural heterogeneity of renal masses quantitatively, and to attempt to discriminate AML without visible fat from ccRCC. In the present study, AML without visible fat could be differentiated from ccRCC with 80%

Table 3
Selected texture features with sequential feature selection (SFS) in each and all four phases of CECT.

CECT phase	Selected texture features	
Unenhanced phase (phase 1)	Mean	Grey-level mean obtained from the histogram
	SD	Grey-level SD obtained from the histogram
	SRE[a]	$\frac{1}{n_r}\sum_{i=1}^{M}\sum_{j=1}^{N}\frac{p(i,j)}{j^2}$
Corticomedullary phase (phase 2)	Std	Grey-level SD obtained from the histogram
	Clt. Prom[b]	$\sum_{i=1}^{N_g}\sum_{j=1}^{N_g}(i+j-u_x-y)^4p(i,j)$
Nephrographic phase (phase 3)	Std	Grey-level SD obtained from the histogram
	Entropy[b]	$-\sum_{i=1}^{N_g}\sum_{j=1}^{N_g}p(i,j)\log(p(i,j))$
	Sum entropy[b]	$-\sum_{i=1}^{2N_g}p_{x+y}(i)\log(p_{x+y}(i))$
	Inf M Corr 1	$\frac{HXY-HXY1}{\max(HX,HY)}$
Excretory phase (phase 4)	SD	Grey-level SD obtained from the histogram
	Kurtosis	Grey-level Kurtosis obtained from the histogram
	LGRE[a]	$\frac{1}{n_r}\sum_{i=1}^{M}\sum_{j=1}^{N}\frac{p(i,j)}{i^2}$
All phases	Mean (phase 1)	Grey-level mean obtained from the histogram
	SD (phase 1 & 4)	Grey-level SD obtained from the histogram
	Clt. prom[b] (phase 3)	$\sum_{i=1}^{N_g}\sum_{j=1}^{N_g}(i+j-u_x-y)^4p(i,j)$
	LRHGE[a] (phase 2)	$\frac{1}{n_r}\sum_{i=1}^{M}\sum_{j=1}^{N}p(i,j)i^2j^2$

SRE, short run emphasis; Clt.prom, cluster prominence; Inf M Corr 1, information measure of correlation; LGRE, low grey-level emphasis; LRHGE, long run high grey-level emphasis; AUC, area under the curve.

[a] $p(i,j)$ indicates the number of grey-level runs j pixels long for a given grey level, i= 1,2, …,N_g. Run length emphasis (RLE) matrix size (M,N).

[b] $p(i,j)$ indicates the joint probability of two pixels having particular co-occurring values, i,j= 1,2, …,N_g. r indicates the total number of neighbouring pixel pairs, N_g indicates the number of grey level used. μ_x, μ_y, δ_x, δ_y indicates means and standard deviations of the row and column sums of the co-occurrence matrix.

$$p_x = \sum_{j=1}^{N_g} p(i,j)$$

$$\mathrm{HXY} = -\sum_{i=1}^{N_g}\sum_{j=1}^{N_g} p(i,j)\log(p(i,j)) \text{ , where HX and HY are entropies of } p_x \text{ and } p_y$$

$$\mathrm{HXY1} = -\sum_{i=1}^{N_g}\sum_{j=1}^{N_g} p(i,j)\log(p_x(i)p_y(j))$$

accuracy based on texture analysis of four-phase CECT. In addition, subgroup analysis of each of the four phases demonstrated that either using unenhanced or contrast-enhanced imaging, the diagnostic accuracy for AML without visible fat was favourable (70–80%) and not statistically different compared with those of the combined four-phase CECT. In daily practice, it might be possible for radiologists to discriminate AML without visible fat from ccRCC on unenhanced CT or routine portal phase CT confidently based on texture analysis.

Table 4
Diagnostic performance of texture analysis in the differentiation of AML without visible fat from ccRCC in each and all four phases of CECT.

CECT phase	Sensitivity (%)	Specificity (%)	Accuracy	AUC	*p*-Value
Unenhanced phase (phase 1)	76.5	88	85.1	0.859	<0.001
Corticomedullary phase (phase 2)	64.7	90	83.6	0.715	0.018
Nephrographic phase (phase 3)	76.5	76	79.1	0.781	<0.001
Excretory phase (phase 4)	47.1	96	83.6	0.747	0.001
All phases	82.4	76	85.1	0.853	<0.001

p=0.05 is significant.

Table 5
Pairwise comparison of ROC curves among four CT phases revealed significant difference between unenhanced and corticomedullary phase.

Comparison of CT phases	*Z* statistic	*p*-Value
Unenhanced versus corticomedullary	2.425	0.015
Unenhanced versus nephrographic	1.074	0.283
Unenhanced versus excretory	1.307	0.191
Unenhanced versus all	0.179	0.858
Corticomedullary versus nephrographic	0.807	0.420
Corticomedullary versus excretory	0.280	0.779
Corticomedullary versus all	1.893	0.058
Nephrographic versus excretory	0.408	0.683
Nephrographic versus all	1.133	0.257
Excretory versus all	1.424	0.154

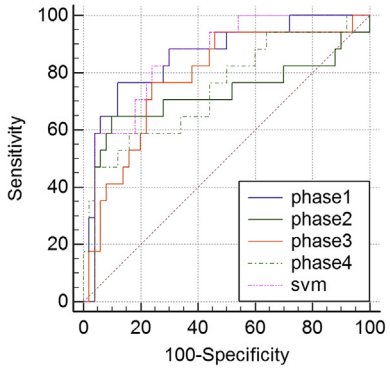

Figure 3 The ROC curves of diagnostic performance in discriminating AML without visible fat and ccRCC. In the subgroup analysis, the AUC was the largest in the unenhanced phase among the four CT phases (AUC: 0.859), although there was no statistically significant difference.

Heterogeneity is one of the characteristics of malignant tumours because it represents intratumoural spatial variations in cellularity, angiogenesis, extravascular extracellular matrix, and areas of necrosis.[17] Tumours with high intratumoural heterogeneity tend to have poorer prognosis and more aggressive biological features.[18] The image interpretation based on visual analysis or random sampling/biopsy may show limited effectiveness for evaluating tissue heterogeneity because these methods are subjective and incomplete or do not represent the full extent of phenotypic or genetic variation within a tumour.[17] Thus, a non-invasive and quantitative method of assessing heterogeneity, i.e., texture analysis might be of clinical benefit.

Several studies of renal lesions have suggested that texture analysis is useful in the differentiation of renal masses.[23,30–33] Texture analysis can be used not only for lesion differentiation, but also for staging and detection of a specific type of RCC. Recently, Hodgdon *et al.* also reported high diagnostic accuracy (AUC: 0.85–0.89) to differentiate between AML and RCC, comparable to the present results (AUC: 0.859 on unenhanced scan)[23]; however, all four CT phases (unenhanced, corticomedullary, nephrographic, and excretory) were examined in the present study whereas Hodgdon *et al.* restricted their study to the analysis of unenhanced imaging. Yan *et al.* reported that unenhanced images showed the best classification result compared with other phases.[30] In the present study, each of the four CT phases showed 70–80% accuracy, with no significant differences between the CT phases except for unenhanced versus corticomedullary phase. The corticomedullary phase showed a significantly lower AUC value (AUC: 0.715) than the unenhanced phase (AUC: 0.859) in the pairwise comparison (p=0.015). This result might be because of the similarly strong arterial enhancement pattern of the two mass groups; however, this result does not have much clinical significance because, in daily clinical practice, CT only in the arterial phase is rarely performed. To the authors' knowledge, the present study is the first to apply quantitative CT texture analysis to diagnose renal masses using four-phase CECT, expanding the result of Hodgdon's study. Although high attenuation on unenhanced CT is an important factor in discriminating AMLs without visible fat,[5,7,10] there were many occasions when patients underwent only contrast-enhanced CT without unenhanced CT in daily clinical practice. In this study, all the CT phases showed reliable diagnostic accuracy (AUC >0.7) regardless of enhancement. Thus, the present results show that with enhanced CT without unenhanced imaging, AML without visible fat can be confidently discriminated from ccRCC using texture analysis.

A limit of 4.5 cm for renal mass size was set in the present study population. As small renal masses tend to lack specific imaging findings for either AML (macroscopic fat) or ccRCC (necrosis, calcification, intratumoural haemorrhage, etc.), it is more difficult to differentiate such masses by visual analysis. Hence, the utility of texture analysis can be maximised in this setting.

ccRCC were included as the control group, unlike in Hodgdon's study. Both ccRCC and AML show similar enhancement patterns, such as strong arterial enhancement and delayed washout, unlike other type of RCCs (chromophobe and papillary RCC). Therefore, the focus was on the differentiation of AML from ccRCC, which was considered to be more difficult to discriminate than other types of RCC.

The present study has several limitations. First, the present study is a retrospective case–control study and can overestimate diagnostic accuracy. Second, the AML group only had 17 participants, which was similar to previous studies on these relatively uncommon renal lesions.[23,30] Third, an imbalance classification issue may arise with the SVM classifier due to discrepant sample sizes in the AML (n=17) and ccRCC (n=50) groups. Leave-one-out cross-validation was performed when performing SVM classification to overcome the problem caused by the differences in the sample size between the two groups. Fourth, two-dimensional (2D) texture analysis was performed on ROIs from one selected representative image instead of three-dimensional (3D) analysis on the entire lesion volume. Full analysis of the 3D tumour volume would allow improved evaluation of intratumoural variations; however, a limit of 4.5 cm was set for tumour size and tumours with necrosis or calcification were excluded. Therefore, a study

population consisting of visually homogeneous renal masses would have minimized intratumoural variations.

In conclusion, the present study showed that quantitative CT texture analysis on four-phase CECT enables superior differentiation of AML without visible fat from ccRCC in comparison to visual analysis. Furthermore, CT texture analysis maintains its diagnostic accuracy in both contrast-enhanced and unenhanced imaging.

Conflict of interest

The authors declare no conflict of interest.

Appendix ASupplementary data

Supplementary data to this article can be found online at https://doi.org/10.1016/j.crad.2019.02.018.

References

1. Zhang YY, Luo S, Liu Y, *et al*. Angiomyolipoma with minimal fat: differentiation from papillary renal cell carcinoma by helical CT. *Clin Radiol* 2013;**68**(4):365–70.
2. Hindman N, Ngo L, Genega EM, *et al*. Angiomyolipoma with minimal fat: can it be differentiated from clear cell renal cell carcinoma by using standard MRI techniques? *Radiology* 2012;**265**(2):468–77.
3. Prasad SR, Surabhi VR, Menias CO, *et al*. Benign renal neoplasms in adults: cross-sectional imaging findings. *AJR Am J Roentgenol* 2008;**190**(1):158–64.
4. Chung MS, Choi HJ, Kim MH, *et al*. Comparison of T2-weighted MRI with and without fat suppression for differentiating renal angiomyolipomas without visible fat from other renal tumours. *AJR Am J Roentgenol* 2014;**202**(4):765–71.
5. Kim JK, Park SY, Shon JH, *et al*. Angiomyolipoma with minimal fat: differentiation from renal cell carcinoma at biphasic helical CT. *Radiology* 2004;**230**(3):677–84.
6. Kim KH, Yun BH, Jung SI, *et al*. Usefulness of the ice-cream cone pattern in computed tomography for prediction of angiomyolipoma in patients with a small renal mass. *Korea J Urol* 2013;**54**(8):504–9.
7. Yang CW, Shen SH, Chang YH, *et al*. Are there useful CT features to differentiate renal cell carcinoma from lipid-poor renal angiomyolipoma? *AJR Am J Roentgenol* 2013;**201**(5):1017–28.
8. Pierorazio PM, Hyams ES, Tsai S, *et al*. Multiphasic enhancement patterns of small renal masses (</=4 cm) on preoperative computed tomography: utility for distinguishing subtypes of renal cell carcinoma, angiomyolipoma, and oncocytoma. *Urology* 2013;**81**(6):1265–71.
9. Kim JK, Kim SH, Jang YJ, *et al*. Renal angiomyolipoma with minimal fat: differentiation from other neoplasms at double-echo chemical shift FLASH MRI imaging. *Radiology* 2006;**239**(1):174–80.
10. Jinzaki M, Tanimoto A, Narimatsu Y, *et al*. Angiomyolipoma: imaging findings in lesions with minimal fat. *Radiology* 1997;**205**(2):497–502.
11. Choi HJ, Kim JK, Ahn H, *et al*. Value of T2-weighted MRI imaging in differentiating low-fat renal angiomyolipomas from other renal tumours. *Acta Radiol* 2011;**52**(3):349–53.
12. Sasiwimonphan K, Takahashi N, Leibovich BC, *et al*. Small (<4 cm) renal mass: differentiation of angiomyolipoma without visible fat from renal cell carcinoma utilizing MRI imaging. *Radiology* 2012;**263**(1):160–8.
13. Sasamori H, Saiki M, Suyama J, *et al*. Utility of apparent diffusion coefficients in the evaluation of solid renal tumours at 3T. *Magn Reson Med Sci* 2014;**13**(2):89–95.
14. Oh TH, Lee YH, Seo IY. Diagnostic efficacy of contrast-enhanced ultrasound for small renal masses. *Korea J Urol* 2014;**55**(9):587–92.
15. Ha SB, Kwak C. Current status of renal biopsy for small renal masses. *Korea J Urol* 2014;**55**(9):568–73.
16. Bayanati H, ET R, Souza CA, *et al*. Quantitative CT texture and shape analysis: can it differentiate benign and malignant mediastinal lymph nodes in patients with primary lung cancer? *Eur Radiol* 2014.
17. Davnall F, Yip CS, Ljungqvist G, *et al*. Assessment of tumour heterogeneity: an emerging imaging tool for clinical practice? *Insights Imaging* 2012;**3**(6):573–89.
18. Ganeshan B, Goh V, Mandeville HC, *et al*. Non-small cell lung cancer: histopathologic correlates for texture parameters at CT. *Radiology* 2013;**266**(1):326–36.
19. Ng F, Ganeshan B, Kozarski R, *et al*. Assessment of primary colorectal cancer heterogeneity by using whole-tumour texture analysis: contrast-enhanced CT texture as a biomarker of 5-year survival. *Radiology* 2013;**266**(1):177–84.
20. Son JY, Lee HY, Lee KS, *et al*. Quantitative CT analysis of pulmonary ground-glass opacity nodules for the distinction of invasive adenocarcinoma from pre-invasive or minimally invasive adenocarcinoma. *PLoS One* 2014;**9**(8):e104066.
21. Chae HD, Park CM, Park SJ, *et al*. Computerized texture analysis of persistent part-solid ground-glass nodules: differentiation of preinvasive lesions from invasive pulmonary adenocarcinomas. *Radiology* 2014:132187.
22. Win T, Miles KA, Janes SM, *et al*. Tumour heterogeneity and permeability as measured on the CT component of PET/CT predict survival in patients with non-small cell lung cancer. *Clin Cancer Res* 2013;**19**(13):3591–9.
23. Hodgdon T, McInnes MD, Schieda N, *et al*. Can quantitative CT texture analysis be used to differentiate fat-poor renal angiomyolipoma from renal cell carcinoma on unenhanced CT images? *Radiology* 2015:142215.
24. Chicklore S, Goh V, Siddique M, *et al*. Quantifying tumour heterogeneity in ^{18}F-FDG PET/CT imaging by texture analysis. *Eur J Nucl Med Mol Imaging* 2013;**40**(1):133–40.
25. Radhakrishnan M, Kuttiannan T, Tiruchengode N. Comparative analysis of feature extraction methods for the classification of prostate cancer from TRUS medical images. *IJCSI Int J Comp Sci Issues* 2012;**9**(1):171–9.
26. Ludmila IK. *A stability index for feature selection. AIAP '07 proceedings of the 25th IASTED international multi-conference: artificial intelligence and applications*. 2007. p. 390–5.
27. Saadi K, Talbot NL, Cawley GC. Optimally regularised kernel Fisher discriminant classification. *Neural Networks* 2007;**20**(7):832–41.
28. Xu D-H, Kurani AS, Furst JD, *et al*. Run-length encoding for volumetric texture. *Heart* 2004;**27**:452–8.
29. Albregtsen F. *Statistical texture measures computed from grey level coocurrence matrices*. Oslo: Image Processing Laboratory, Department of Informatics. University of Oslo; 2008.
30. Yan L, Liu Z, Wang G, *et al*. Angiomyolipoma with minimal fat: differentiation from clear cell renal cell carcinoma and papillary renal cell carcinoma by texture analysis on CT images. *Acad Radiol* 2015;**22**:1115–21.
31. Raman SP, Chen Y, Schroeder JL, *et al*. CT texture analysis of renal masses: pilot study using random forest classification for prediction of pathology. *Academic Radiol* 2014 Dec;**21**(12):1587–96.
32. Kierans AS, Rusinek H, Lee A, *et al*. Textural differences in apparent diffusion coefficient between low- and high-stage clear cell renal cell carcinoma. *AJR Am J Roentgenol* 2014;**203**(6):W637–44.
33. Schieda N, Thornhill RE, Al-Subhi M, *et al*. Diagnosis of sarcomatoid renal cell carcinoma with CT: evaluation by qualitative imaging features and texture analysis. *AJR Am J Roentgenol* 2015;**204**(5):1013–23.